Aberrant Nuclear Export of circNCOR1 Underlies SMAD7-Mediated Lymph Node Metastasis of Bladder Cancer

Mingjie An[1,2,3], Hanhao Zheng[1,2,3], Jian Huang[1,2,3], Yan Lin[1,2,3], Yuming Luo[4], Yao Kong[4], Mingrui Pang[1,2,3], Dingwen Zhang[4,5], Jiabin Yang[4,5], Jiancheng Chen[1,2,3], Yuanlong Li[1,2,3], Changhao Chen[1,2,3], and Tianxin Lin[1,2,3]

ABSTRACT

Circular RNAs (circRNA) containing retained introns are normally sequestered in the nucleus. Dysregulation of cellular homeostasis can drive their nuclear export, which may be involved in cancer metastasis. However, the mechanism underlying circRNA nuclear export and its role in lymph node (LN) metastasis of bladder cancer remain unclear. Here, we identify an intron-retained circRNA, circNCOR1, that is significantly downregulated in LN metastatic bladder cancer and is negatively associated with poor prognosis of patients. Overexpression of circNCOR1 inhibited lymphangiogenesis and LN metastasis of bladder cancer *in vitro* and *in vivo*. Nuclear circNCOR1 epigenetically promoted SMAD7 transcription by increasing heterogeneous nuclear ribonucleoprotein L (hnRNPL)–induced H3K9 acetylation in the SMAD7 promoter, leading to inhibition of the TGFβ-SMAD signaling pathway. Nuclear retention of circNCOR1 was regulated by small ubiquitin-like modifier (SUMO)ylation of DDX39B, an essential regulatory factor responsible for circRNA nuclear-cytoplasmic transport. Reduced SUMO2 binding to DDX39B markedly increased circNCOR1 retention in the nucleus to suppress bladder cancer LN metastasis. By contrast, SUMOylated DDX39B activated nuclear export of circNCOR1, impairing the suppressive role of circNCOR1 on TGFβ-SMAD cascade activation and bladder cancer LN metastasis. In patient-derived xenograft (PDX) models, overexpression of circNCOR1 and inhibition of TGFβ signaling significantly repressed tumor growth and LN metastasis. This study highlights SUMOylation-induced nuclear export of circNCOR1 as a key event regulating TGFβ-SMAD signaling and bladder cancer lymphangiogenesis, thus supporting circNCOR1 as a novel therapeutic agent for patients with LN metastatic bladder cancer.

Significance: This study identifies the novel intron-retained circNCOR1 and elucidates a SUMOylation-mediated DDX39B–circNCOR1–SMAD7 axis that regulates lymph node metastasis of bladder cancer.

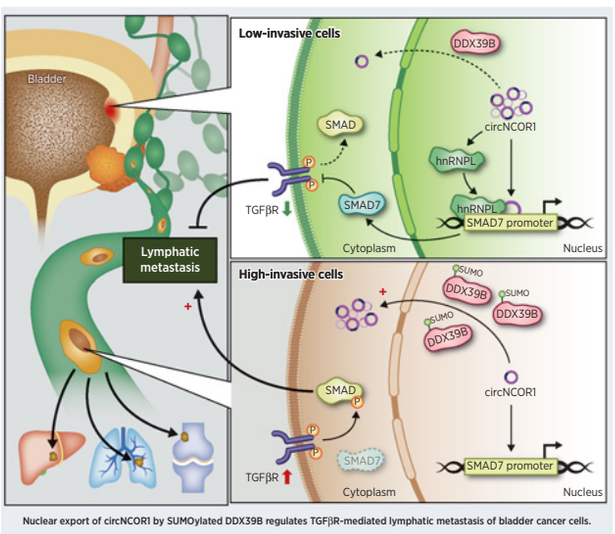

Nuclear export of circNCOR1 by SUMOylated DDX39B regulates TGFβR-mediated lymphatic metastasis of bladder cancer cells.

Introduction

Bladder cancer is the most prevalent oncological disease contributing to genitourinary system cancer-related deaths, with approximately 524,000 new cases and 229,000 deaths annually (1, 2). Among the diverse lethal factors, lymph node (LN) metastasis is considered the leading cause for the poor prognosis of bladder cancer, reducing the 5-year survival rate of patients to less than 20% (3, 4). Many researchers have proposed that lymphangiogenesis, the generation of neonatal lymphatic vessels from preexisting lymphatic networks, is the essential

[1]Department of Urology, Sun Yat-sen Memorial Hospital, Sun Yat-sen University, Guangzhou, Guangdong, China. [2]Guangdong Provincial Key Laboratory of Malignant Tumor Epigenetics and Gene Regulation, Medical Research Center, Sun Yat-sen Memorial Hospital, Sun Yat-sen University, Guangzhou, Guangdong, China. [3]State Key Laboratory of Oncology in South China, Sun Yat-sen University Cancer Center, Guangzhou, Guangdong, China. [4]Pancreatic Center, Department of General Surgery, Guangdong Provincial People's Hospital, Guangdong Academy of Medical Sciences, Guangzhou, Guangdong, China. [5]School of Medicine, South China University of Technology, Guangzhou, Guangdong, China.

Note: Supplementary data for this article are available at Cancer Research Online (http://cancerres.aacrjournals.org/).

M. An, H. Zheng, and J. Huang contributed equally to this article.

Corresponding Authors: Tianxin Lin, Department of Urology, Sun Yat-sen Memorial Hospital, Sun Yat-sen University, 107 Yanjiangyi Road, Yuexiu District, Guangzhou, Guangdong Province 510120, P. R. China. Phone: 8620-3407-0447; Fax: 8620-8133-2336; E-mail: lintx@mail.sysu.edu.cn; and Changhao Chen, chenchh53@mail.sysu.edu.cn

Cancer Res 2022;82:2239–53

doi: 10.1158/0008-5472.CAN-21-4349

and limiting process of bladder cancer LN metastasis (5, 6). Uncontrolled sprouting of lymphatic vessels in the tumor microenvironment forms a potential route for tumor cell invasion into the lymph drainage system, resulting in the accumulation of intravascular cancer embolus and predicting tumor recurrence and metastasis (7, 8). Accordingly, fully characterizing the molecular mediators and regulatory mechanisms governing tumor lymphangiogenesis are of great clinical importance for patients with bladder cancer.

Circular RNAs (circRNA) are covalently closed RNA molecules involved in regulating tumor metastasis by inducing tumor cell epithelial–mesenchymal transition (EMT), stemness, and immune escape (9–11). The majority of annotated back-splicing circRNAs are primarily located in the cytoplasm, while several circRNAs with retained introns are sequestered in the nucleus (12, 13). It has been proposed that cancer malignant transformation is frequently accompanied by the balanced weakening of circRNA subcellular localization, leading to the increment of nuclear exportation (14, 15). Intensive researches have demonstrated that aberrant circRNA nuclear exportation contributes to the dysregulation of intracellular signaling transduction, allowing tumor cells to acquire the aggressive phenotypes and activating the tumor metastatic cascade (16, 17). However, the mechanisms underlying circRNA nuclear exportation in bladder cancer LN metastasis remain largely unclear.

DDX39B is an evolutionarily conserved member of the DExD-box helicase family required for mediating the metabolism processing of multiple cellular RNAs, including pre-mRNA transcription, splicing, and nuclear export (18, 19). It has been verified that DDX39B acts as a mediator of circRNA subcellular trafficking in a length-dependent manner, where it induces the nuclear exportation of longer circRNAs (20, 21). The pattern of length controlling circRNA nuclear exportation is subject to certain limitations to the mechanism of DDX39B recognition and recruitment of circRNAs with specific lengths (22). Studies on protein three-dimensional structures have revealed that DDX39B acts as a vital oncogene and is characterized by several surface-exposed lysine (K) residues to present a variety of posttranslational modifications (PTM) crucial for RNA nuclear exportation (23, 24). However, the regulatory mechanisms of DDX39B, with specific PTMs mediating circRNA nuclear exportation to trigger bladder cancer LN metastasis, remain unknown.

In this study, we identified an intron-retained circRNA, circNCOR1 (hsa_circ_0042174), which was downregulated in bladder cancer and correlated negatively with LN metastasis in patients with bladder cancer. Overexpressing circNCOR1 markedly suppressed lymphangiogenesis and LN metastasis of bladder cancer *in vitro* and *in vivo*. Moreover, decreasing small ubiquitin-like modifier 2 (SUMO2) modification of DDX39B significantly impaired circNCOR1 nuclear exportation to inhibit bladder cancer LN metastasis. Mechanistically, nuclear circNCOR1 recruited heterogeneous nuclear ribonucleoprotein L (hnRNPL) to the SMAD family member 7 (*SMAD7*) promoter and epigenetically activated *SMAD7* transcription by increasing H3K9 acetylation on the *SMAD7* promoter, thereby inhibiting TGFβ–SMAD signaling, while SUMOylated DDX39B induced circNCOR1 nuclear exportation to impair its inhibitory role in bladder cancer LN metastasis. Furthermore, we conducted experimental treatment in patient-derived xenograft (PDX) models and demonstrated that circNCOR1 may be a potential therapeutic inhibitor of bladder cancer. Our study reveals the underlying mechanism of circNCOR1 nuclear exportation, indicating that targeting circRNA nuclear exportation might be a potential therapeutic target for treating LN metastatic bladder cancer.

Materials and Methods

Clinical samples and ethics statement

A total of 228 pairs of bladder cancer tissues and noncancerous adjacent tissues (NAT) were obtained from patients who had undergone surgical resection at Sun Yat-sen Memorial Hospital of Sun Yat-sen University (Guangzhou, Guangdong, China). The histologic and pathologic type of each clinical sample was diagnosed by three experienced pathologists independently. The specimens were obtained with the written informed consent of all patients and was approved by the Ethics Committees of Sun Yat-sen Memorial Hospital of Sun Yat-sen University [approval number: 2013(61)]. The studies were conducted in accordance with recognized ethical guidelines. Supplementary Table S1 summarizes the patients' detailed clinical and pathologic data.

Cell lines and cell culture

The human urinary bladder transitional cell carcinoma cell lines T24 (RRID: CVCL_0554), UM-UC-3 (RRID: CVCL_1783) were purchased from ATCC, RT112 (RRID: CVCL_1670) was purchased from German Collection of Microorganisms and Cell Cultures GmbH (DSMZ) and UM-UC-1 (RRID: CVCL_2743) was purchased from European Collection of Authenticated Cell Cultures (ECACC). Human normal bladder epithelial cell line SV-HUC-1 (RRID: CVCL_3798) was purchased from ATCC. Murine transitional cell carcinoma cell line MB49 (RRID: CVCL_7076) was purchased from Millipore, and murine bladder epithelial cells (MBEC) were purchased from Procell (catalog no. CP-M058). Human lymphatic endothelial cells (HLEC) were obtained from ScienCell Research Laboratories. All cells were maintained in a humidified incubator with 5% CO_2 at 37°C. The T24, RT112, and UM-UC-1 cells were cultured in RPMI 1640 medium (Gibco, catalog no. C11875500BT). The UM-UC-3 and MB49 cells were cultured in DMEM (Gibco, catalog no. C11995500BT). The SV-HUC-1 cells were cultured in Ham's F12K medium (Gibco, catalog no. 21127022). All medium was supplemented with 10% FBS (BI, catalog no. 04–001–1ACS). The HLECs were cultured in endothelial cell medium (ECM) with 5% FBS (ScienCell Research Laboratories, catalog no. 1001). The authentication and *Mycoplasma* testing of all cell lines were qualified.

Mouse popliteal lymphatic metastasis model

A mouse popliteal lymphatic metastasis model was constructed to explore the role of circNCOR1 in bladder cancer LN metastasis. BALB/c nude mice and C57BL/6 mice (approximately 4–5 weeks old) were purchased and kept at the Experimental Animal Center, Sun Yat-sen University and used to construct the footpad tumor model as described in our previous study (25). Briefly, 5×10^5 GFP-labeled UM-UC-3 and MB49 cells were harvested and resuspended in 20 μL PBS, and were slowly injected into the footpads of the mice. Popliteal LN metastasis was monitored weekly by *In Vivo* Imaging Systems (IVIS; Xenogen Corporation) until the footpad tumor was 200 mm^3. Then, the footpad tumors and popliteal LNs were dissected and paraffin-embedded for IHC detection. Animal experiments were performed with the approval of the Sun Yat-sen University Institutional Animal Care and Use Committee (IACUC) and the animals were handled in accordance with institutional guidelines.

Establishment and treatment of mice carrying PDXs

The PDX mouse model was established to determine the therapeutic effect of circNCOR1. Fresh bladder cancer samples obtained from 2 patients who had undergone surgery at Sun Yat-sen Memorial Hospital of Sun Yat-sen University were implanted as subcutaneous

tumors in 4-week-old NOD/SCID/IL2rγ-null (NSG) mice (first generation, F1). Xenografts from the F1 mice were cut into pieces and transplanted into F2 mice. When the tumors were 1.5 cm^3, they were excised and divided into pieces in equal volumes and transplanted into F3 mice. When the PDXs were about 200 mm^3, the F3 mice were randomly divided into several groups ($n = 6$ per group) and treated with intratumoral injection of *in vivo*–optimized circNCOR1 lentivirus, LY2157299 (Selleck, catalog no. S2230), siTGFBR1 and siSMAD7 (RiboBio), respectively. The tumor volume was calculated as 0.5 × length × $width^2$ and monitored every 3 days. All mice were killed 36 days after treatment and the PDX tumors were analyzed. Animal experiments were performed with the approval of the Sun Yat-sen University IACUC and the animals were handled in accordance with institutional guidelines.

CRISPR-Cas9–mediated gene deletion

LentiCRISPR v2 vectors containing single-guide RNAs targeting *DDX39B* were purchased from UBIgene and transfected into UM-UC-3 and T24 cells to construct the *DDX39B* knockout (KO) bladder cancer cells as described previously (7). The KO efficiency was evaluated with qRT-PCR analysis.

Statistical analysis

All statistical analyses were performed using SPSS (IBM Corp., RRID:SCR_002865). All quantitative data are expressed as the average SD of at least three independent experiments. Data with statistical differences were identified using the χ^2 test for nonparametric variables and with Student *t* test (two-tailed) and ANOVA for parametric variables. Statistical significance for IHC analyses was assessed using the *H*-score. The correlation between groups was analyzed with Pearson correlation analysis. Overall survival (OS) and disease-free survival (DFS) were calculated with Kaplan–Meier survival analysis. The HR and 95% confidence interval for identifying independent prognostic factors were estimated with the multivariate Cox regression model. In all statistical analyses, $P < 0.05$ was defined as the threshold for statistical significance.

Data availability

More detailed methods are available in the Supplementary Materials and Methods. The data generated in this study are available within the article and its Supplementary data files. The sequencing data generated from this study are publicly available in Gene Expression Omnibus (GEO; RRID:SCR_005012) at GSE191036, GSE77661, GSE190827.

Results

circNCOR1 is negatively associated with bladder cancer LN metastasis

LN metastasis represents a major cause of cancer-related mortality and preventing it improves the prognosis of patients with bladder cancer (26). To identify the critical circRNAs involved in inhibiting bladder cancer LN metastasis, we first conducted next-generation sequencing (NGS) of four paired bladder cancer tissues and NATs (GSE191036; **Fig. 1A**). Then, we analyzed the RNA sequencing (RNA-seq) data from a public GEO dataset (GSE77661) of bladder cancer tissues and paired NATs to identify the downregulated circRNAs. As tumor cell invasiveness marks the metastatic characteristic of tumor, we established an invasion model to screen the crucial circRNAs contributing to bladder cancer aggressiveness and metastasis (**Fig. 1B**). The intersection of these three sequencing experiments identified seven circRNAs as consistently downregulated in both high-invasive bladder cancer cells and bladder cancer tissues (**Fig. 1C**). Next, we evaluated the correlation between the expression levels of these seven circRNAs and bladder cancer LN metastatic status in our 228-case clinical cohort to confirm that circNCOR1 (hsa_circ_0042174) was the most significantly downregulated circRNA in bladder cancer tissues compared with NATs and in LN metastatic bladder cancer tissues compared with those without LN metastasis (**Fig. 1D** and **E**). Strikingly, IHC staining of lymphatic vessel endothelial hyaluronan receptor 1 (LYVE-1) showed that circNCOR1 overexpression was negatively associated with microlymphatic vessel density (MLD) in both intratumoral and peritumoral regions in the bladder cancer tissues (**Fig. 1F** and **G**), indicating that circNCOR1 inhibits bladder cancer lymphangiogenesis. Importantly, Kaplan–Meier analysis using the median as cutoff showed that low circNCOR1 expression was related to poor OS and DFS in patients with bladder cancer (**Fig. 1H** and **I**). Univariate and multivariate Cox analyses demonstrated that circNCOR1 was an independent prognostic factor for the patients' OS and DFS (Supplementary Table S2 and S3). Collectively, these results demonstrate that circNCOR1 is negatively associated with LN metastasis and better prognosis of patients with bladder cancer.

Identification of circNCOR1 characteristics

As the back-splicing of specific exons and introns for circRNA formation determines their subcellular localization and biological function (27), we evaluated the mature sequence of circNCOR1, which has a residual fragment of intron 18 and the entire exon 19 from the *NCOR1* gene, being 556-nucleotides (nt) long (**Fig. 1J** and **K**). Using cDNA and genomic DNA (gDNA) from bladder cancer cells as templates, divergent primers amplified circNCOR1 only in the cDNA groups rather than in the gDNA groups (**Fig. 1L**; Supplementary Fig. S1A). Moreover, circNCOR1 was difficult to reverse-transcribe into cDNA using oligo-dT primers as compared with random primers (**Fig. 1M**), indicating that it has a circular structure without a poly (A) tailed structure. Treatment with RNase R, an exoribonuclease that degrades linear mRNA, significantly decreased the linear *NCOR1* mRNA levels while no variation was observed for circNCOR1 (**Fig. 1N**), confirming its closed circular form. Consistent with this, circNCOR1 exhibited a significantly longer half-life than *NCOR1* mRNA in bladder cancer cells after actinomycin D treatment (**Fig. 1O**; Supplementary Fig. S1B). Taken together, these findings demonstrate that circNCOR1 is a highly stable and intron-retained circRNA.

SUMOylated DDX39B promotes circNCOR1 nuclear exportation

Interestingly, RNA *in situ* hybridization (ISH) of the clinical samples revealed two distinct staining patterns, in which circNCOR1 was mainly enriched in the nucleus of low-grade bladder cancer but was significantly detected in the cytoplasmic regions of high-grade bladder cancer (**Fig. 2A** and **B**), indicating differential subcellular location of circNCOR1 between low- and high-grade bladder cancer specimens. Furthermore, the RNA FISH and subcellular fraction assays of the bladder cancer cell lines demonstrated that the vast majority of circNCOR1 was located in the nucleus of UM-UC-1, RT112 and established low-invasive cells, while it was mostly detected in the cytoplasm of UM-UC-3, T24 and established high-invasive cells (**Fig. 2C** and **D**; Supplementary Fig. S1C), indicating discrepant subcellular localization of circNCOR1 in low and high-grade bladder cancer. As the DDX39 family, including DDX39A and DDX39B, are essential regulatory factors responsible for circRNA nuclear–cytoplasmic transportation (20), we first evaluated whether DDX39A

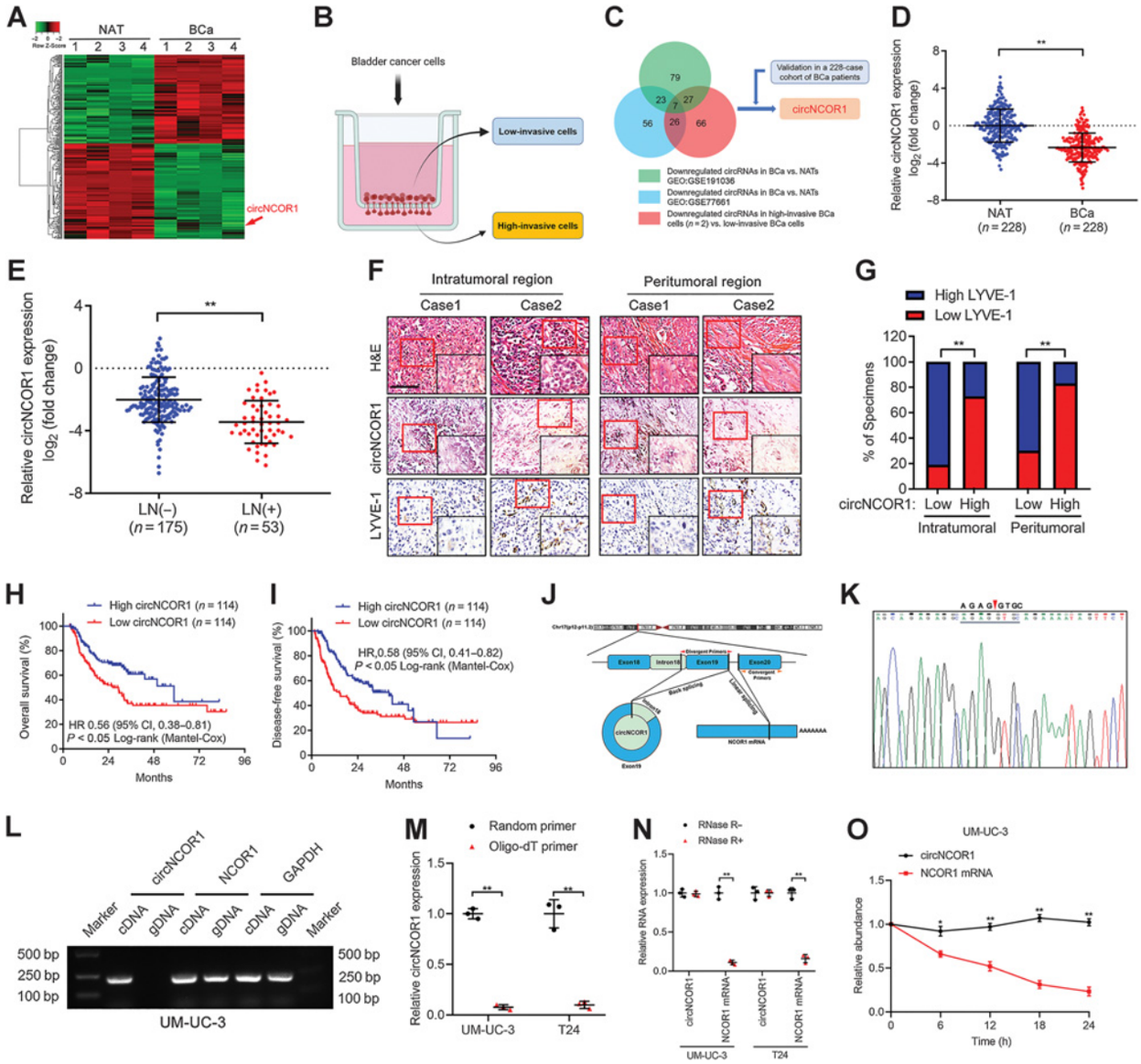

Figure 1.

circNCOR1 downregulation is negatively associated with LN metastasis of bladder cancer. **A,** Heatmap of the circRNAs differentially expressed in bladder cancer (BCa) tissues compared with NATs. **B,** Schematic representation showing the establishment of high- and low-invasive bladder cancer cell lines. **C,** Schematic illustration for screening the codownregulated circRNAs in bladder cancer tissues and high-invasive bladder cancer cells. **D** and **E,** qRT-PCR analysis of circNCOR1 expression in bladder cancer tissues versus NATs (**D**) and LN-positive versus LN-negative bladder cancer tissues (**E**; $n = 228$). **F** and **G,** Representative images (**F**) and percentages (**G**) of circNCOR1 expression and LYVE-1–indicated lymphatic vessels in bladder cancer tissues. Scale bars, 50 μm. **H** and **I,** Kaplan–Meier survival analysis of the OS (**H**) and DFS (**I**) of patients with bladder cancer with low versus high circNCOR1 expression. The cutoff is the median. **J,** Schematic illustrating the genetic locus of the *NCOR1* gene and circNCOR1 derived from intron 18 to exon 19 of *NCOR1*. **K,** The back-splicing junction of circNCOR1 was identified by Sanger sequencing. **L,** PCR with agarose gel electrophoresis assay of circNCOR1 and *NCOR1* in the cDNA and gDNA of UM-UC-3 cells. **M,** qRT-PCR analysis of circNCOR1 expression using random primers or oligo-dT primers. **N,** qRT-PCR analysis of circNCOR1 and *NCOR1* expression in bladder cancer cells treated with or without RNase R. **O,** Assessment of circNCOR1 and *NCOR1* mRNA stability in UM-UC-3 cells. The statistical difference was assessed through the nonparametric Mann–Whitney *U* test in **D**, **E**, **H**, and **I** and the χ^2 test in **G**; and the two-tailed Student *t* test in **M–O**. Error bars show the SD from three independent experiments. *, $P < 0.05$; **, $P < 0.01$.

and DDX39B regulate the subcellular localization of circNCOR1 in bladder cancer cells. The subcellular fraction assays revealed that overexpressing *DDX39A* failed to mediate circNCOR1 nuclear exportation (Supplementary Fig. S1D–S1K), but overexpressing *DDX39B* increased the cytoplasmic accumulation of circNCOR1, while downregulating *DDX39B* attenuated circNCOR1 nuclear exportation in UM-UC-3 cells (**Fig. 2E**). There was no statistical difference for circNCOR1 localization in UM-UC-1 cells after *DDX39B* expression levels had been altered (**Fig. 2F**; Supplementary Fig. S1 L–Q), suggesting that DDX39B may exhibit particular biological features in high-invasive bladder cancer cells. Accordingly, we focused on the specific mechanism underlying DDX39B-mediated circNCOR1 nuclear

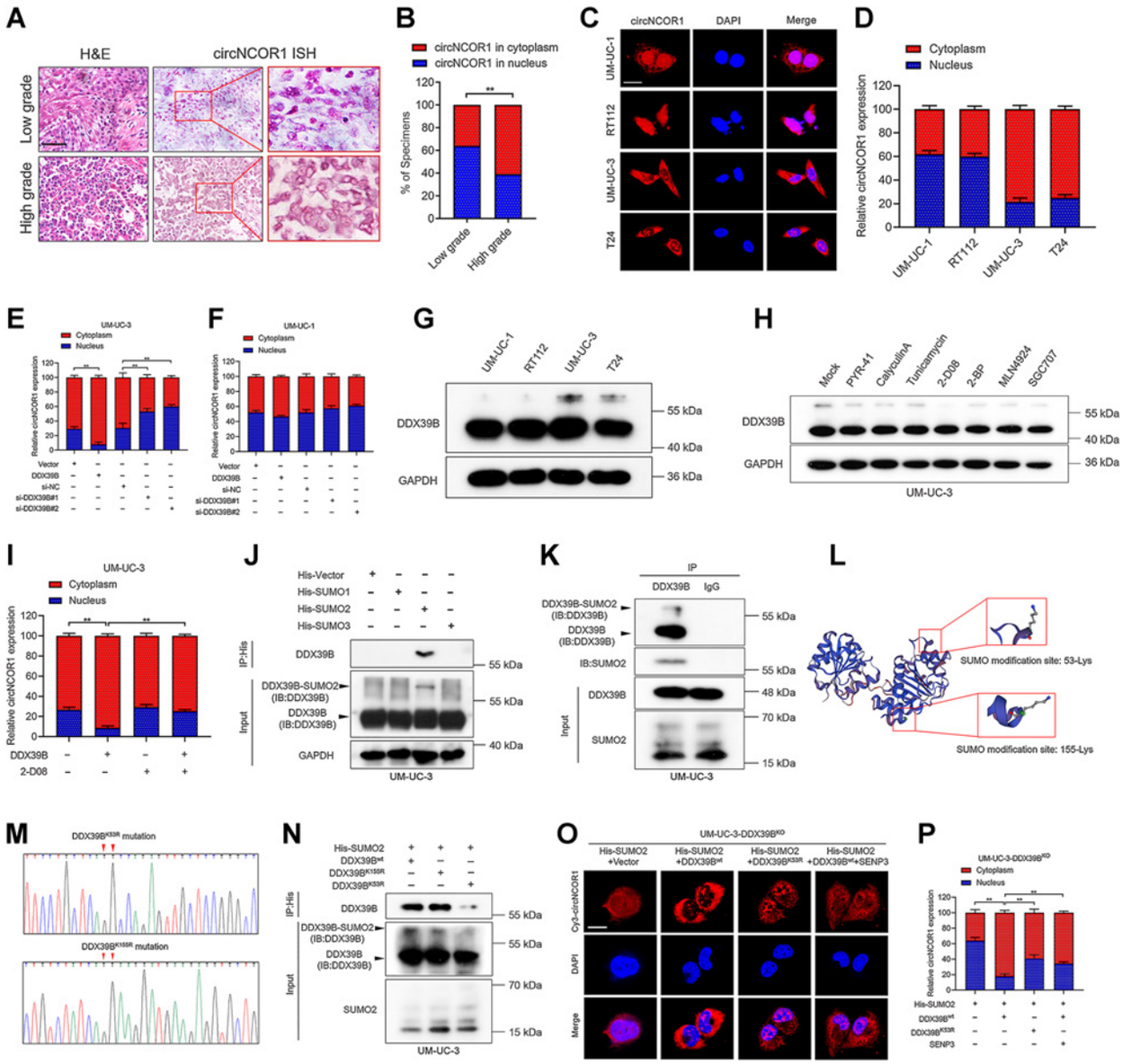

Figure 2.

SUMOylation promotes DDX39B-mediated circNCOR1 nuclear exportation. **A** and **B,** Representative images (**A**) and histogram (**B**) of circNCOR1 location in low- and high-grade bladder cancer tissues. Scale bars, 50 μm. H&E, hematoxylin and eosin. **C** and **D,** FISH (**C**) and subcellular fraction analysis (**D**) of circNCOR1 cellular localization in bladder cancer cells. Scale bars, 5 μm. **E** and **F,** Subcellular fraction analysis of circNCOR1 in UM-UC-3 (**E**) and UM-UC-1 (**F**) cells after overexpressing or downregulating *DDX39B*. **G,** Western blotting verified the PTM of DDX39B in bladder cancer cells. **H,** Western blotting of the PTM level of DDX39B after inhibitor treatment in UM-UC-3 cells. **I,** Subcellular fraction analysis of circNCOR1 cellular localization in indicated UM-UC-3 cells. **J,** Western blotting of the SUMOylation type of DDX39B in UM-UC-3 cells. **K,** Western blotting verified the SUMO2 modification of DDX39B after coimmunoprecipitation with anti-DDX39B and IgG control in UM-UC-3 cells. **L,** Schematic illustration of the SUMOylation sites on DDX39B predicted by GPS-SUMO. **M,** Sanger sequencing evaluation of the DDX39B^{K53R} and DDX39B^{K155R} mutations. **N,** Western blotting verified that the SUMO2 modification site of DDX39B was the K53 residue. **O** and **P,** FISH (**O**) and subcellular fraction analysis (**P**) of circNCOR1 in indicated UM-UC-3 cells. Scale bars, 5 μm. The statistical difference was assessed with the χ^2 test in **B**, **E**, **F**, **I**, and **P**. Error bars show the SD from three independent experiments. **, $P < 0.01$.

exportation in high-invasive bladder cancer cells. Western blotting showed that DDX39B had an additional band with a higher molecular weight that was markedly overexpressed in UM-UC-3 and T24 cells (**Fig. 2G**; Supplementary Fig. S2A and S2B), indicating that it has a higher level of PTM in high-invasive bladder cancer cells.

To determine the specific PTM type of DDX39B, Western blotting was performed for bladder cancer cells that had been treated with inhibitors targeting different types of PTM, and the treatment with 2-D08, a comprehensive SUMOylation inhibitor, significantly attenuated the PTM level of DDX39B (**Fig. 2H**; Supplementary Fig. S2C–S2G), indicating that DDX39B was SUMOylated in bladder cancer. Moreover, the subcellular fraction assays revealed that 2-D08 markedly impaired the DDX39B-induced circNCOR1 nuclear exportation in bladder cancer cells (**Fig. 2I**; Supplementary Fig. S2H), indicating that

SUMOylation is indispensable for DDX39B-mediated circNCOR1 nuclear exportation.

To verify the SUMOylation type of DDX39B, UM-UC-3 cell lines stably expressing His-tagged SUMO1, SUMO2, and SUMO3 were constructed and subjected to coimmunoprecipitation assays using anti-His antibody. DDX39B was detected only in the His-SUMO2 overexpressing cells (**Fig. 2J**; Supplementary Fig. S2I). Consistently, an additional band of SUMO2-modified DDX39B was observed at 55 kDa above, which was the theoretical molecular weight of DDX39B conjugated with SUMO2 (**Fig. 2K**; Supplementary Fig. S2J), confirming that DDX39B was SUMOylated with SUMO2 in UM-UC-3 cells. Given that the modification residues are essential for determining the biological role of SUMOylation on its target proteins, we used GPS-SUMO, a tool for SUMOylation site analysis, to predict two potential SUMO modification sites of DDX39B: K53 and K155 (**Fig. 2L**; Supplementary Fig. S2K). Subsequently, these potential sites were substituted with arginine (R; DDX39B^{K53R} and DDX39B^{K155R}) to show that DDX39B^{K53R} rather than DDX39B^{K155R} dramatically reduced the SUMO2 modification level of DDX39B (**Fig. 2M** and **N**; Supplementary Fig. S2L), demonstrating that the K53 residue was the major SUMOylation site of DDX39B.

We used the CRISPR-Cas9 system to examine whether SUMOylation regulates DDX39B-mediated circNCOR1 nuclear exportation, and successfully silenced *DDX39B* expression in high-invasive bladder cancer cells to eliminate the effect of endogenous DDX39B in regulating circNCOR1 subcellular localization (Supplementary Fig. S2M–S2O). Notably, *DDX39B* overexpression in UM-UC-3-DDX39B^{KO} (*DDX39B* KO) cells facilitated circNCOR1 nuclear exportation, and upregulating SUMO2 markedly enhanced the efficiency of DDX39B-mediated circNCOR1 nuclear exporting. Meanwhile, the K53R mutation or the overexpression of SENP3 (SUMO-specific peptidase 3), a deSUMOylase mainly targeting SUMO2 conjunction, markedly reduced the SUMO2 modification of DDX39B to inhibit circNCOR1 nuclear exportation (**Fig. 2O** and **P**; Supplementary Fig. S2P and S2Q). Together, these findings demonstrate that DDX39B is SUMOylated with SUMO2 at K53 and that SUMO2 modification promotes DDX39B-mediated circNCOR1 nuclear exportation.

circNCOR1 suppresses lymphangiogenesis of bladder cancer *in vitro*

Since circNCOR1 was clinically associated with bladder cancer LN metastasis, we determined the biological function of circNCOR1 in bladder cancer by gain- and loss-of-function assays *in vitro*. First, circNCOR1 expression evaluation of human normal bladder epithelial cells (SV-HUC-1) and the bladder cancer cell lines revealed that UM-UC-3 and T24 cells had the lowest circNCOR1 expression (Supplementary Fig. S3A). Then, we successfully altered circNCOR1 expression via transfection with siRNAs or circNCOR1 plasmid, whereas no obvious change in *NCOR1* mRNA level was observed (Supplementary Fig. S3B–E).

Given that many have proposed that lymphangiogenesis is the crucial step in tumor LN metastasis, we explored the effect of circNCOR1 on bladder cancer lymphangiogenesis by coculturing HLECs with bladder cancer cells. Coculture with circNCOR1-downregulated UM-UC-3 and T24 cells markedly promoted HLECs tube formation and migration as compared with the control. Conversely, HLECs tube formation and migration were markedly inhibited after coculture with circNCOR1-overexpressing UM-UC-3 and T24 cells (**Fig. 3A**; Supplementary Fig. S3F), indicating that circNCOR1 suppresses lymphangiogenesis of bladder cancer *in vitro*.

Tumor LN metastasis is an elaborate multistep process regulated by various elements. In addition to the formation of the neonatal lymphatic network induced by tumor cell-secreted lymphangiogenic factors, enhanced tumor cells invasiveness is also vital for stimulating tumor LN metastasis. Therefore, we investigated the biological function of circNCOR1 in bladder cancer cells invasiveness. Transwell and wound healing assays revealed that downregulating circNCOR1 enhanced UM-UC-3 and T24 cell migration and invasion, whereas overexpressing circNCOR1 had the opposite effect (Supplementary Fig. S3G–S3J). Collectively, our results indicate that circNCOR1 overexpression suppresses lymphangiogenesis of bladder cancer *in vitro*.

circNCOR1 inhibits LN metastasis of bladder cancer *in vivo*

To further examine the effect of circNCOR1 on bladder cancer LN metastasis *in vivo*, a popliteal LN metastatic model was constructed by implanting GFP-labeled circNCOR1-overexpressing UM-UC-3 cells into the footpads of nude mice as described previously (28). IVIS showed that circNCOR1 overexpression decreased the fluorescence intensity of the popliteal LNs remarkably as compared with the control (**Fig. 3B**), indicating that circNCOR1 inhibits bladder cancer cell metastasis to the popliteal LNs of the nude mice. Furthermore, enucleating the popliteal LNs for IVIS and IHC analyses revealed a lower metastatic rate of LNs in the circNCOR1-overexpressing group than in the control group (**Fig. 3C–F**). Strikingly, circNCOR1 overexpression significantly reduced the LYVE-1-indicated MLD in both the intratumoral and peritumoral regions of the footpad primary tumor tissues (**Fig. 3G** and **H**), confirming that circNCOR1 suppresses lymphangiogenesis of bladder cancer. Considering that immune cells also play a major role in LN metastasis, we implanted GFP-labeled circNCOR1-overexpressing MB49 cells into the footpads of C57BL/6 mice to evaluate the effect of circNCOR1 on LN metastasis in immunocompetent model. The results revealed that circNCOR1 overexpression markedly decreased the fluorescence intensity and LN metastatic rate of the popliteal LNs in C57BL/6 mice (Supplementary Fig. S4A–S4G). Together, these findings demonstrate that circNCOR1 inhibits lymphangiogenesis and LN metastasis of bladder cancer *in vivo*.

SUMOylated DDX39B mediates nuclear exportation of circNCOR1 to promote bladder cancer LN metastasis

Since our results verified that SUMOylated DDX39B mediated circNCOR1 nuclear exportation, we explored whether circNCOR1 nuclear exportation was involved in regulating bladder cancer LN metastasis. Overexpressing *DDX39B* reversed the inhibition of HLECs tube formation and migration induced by circNCOR1 overexpression in UM-UC-3 cells, while muting K53 in DDX39B (DDX39B^{K53R}) or SENP3 treatment impaired this effect (**Fig. 4A–C**), indicating that DDX39B-mediated circNCOR1 nuclear exportation promotes bladder cancer lymphangiogenesis *in vitro*. Similarly, IVIS showed that *DDX39B* overexpression retrieved the circNCOR1-mediated reduction of popliteal LN fluorescence intensity in the nude mice. Conversely, DDX39B^{K53R} or SENP3 treatment significantly abrogated the *DDX39B* overexpression-enhanced UM-UC-3 cells metastasis to the popliteal LNs (**Fig. 4D–F**). Furthermore, the LN metastasis rate was significantly increased in the *DDX39B* overexpression group compared with the control, while DDX39B^{K53R} or SENP3 treatment markedly rescued the circNCOR1-mediated inhibition of bladder cancer LN metastasis *in vivo* (**Fig. 4G**). Importantly, IHC staining demonstrated that *DDX39B* overexpression significantly reversed the circNCOR1-mediated reduction of MLD in both the intratumoral and peritumoral regions of the footpad primary tumor tissues, while

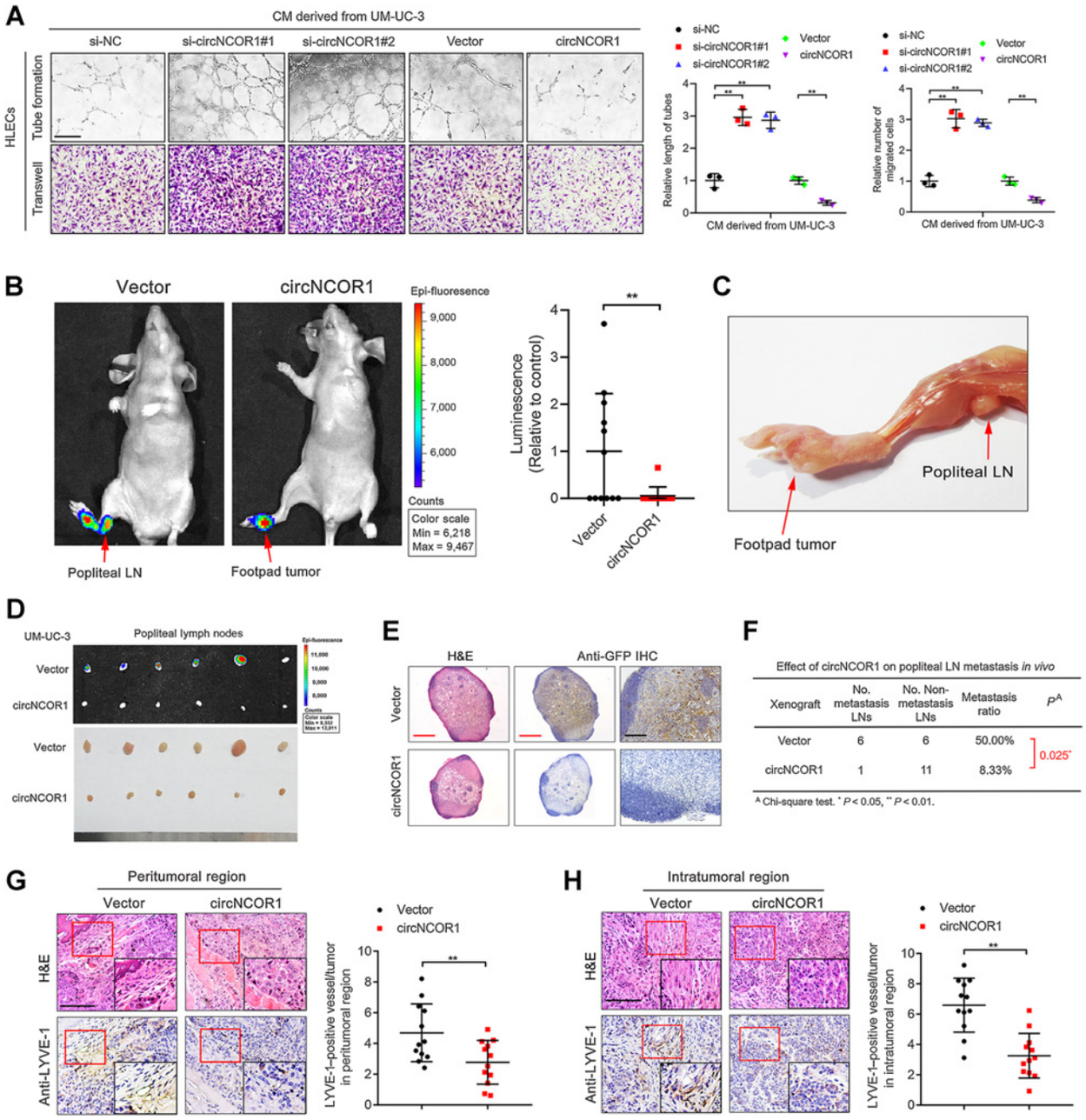

Figure 3.

circNCOR1 suppresses lymphangiogenesis and LN metastasis of bladder cancer *in vitro* and *in vivo*. **A,** Representative images and quantification of tube formation and Transwell migration of HLECs cocultured with circNCOR1-downregulated or -overexpressing UM-UC-3 cells. Scale bars, 100 μm. **B,** Representative bioluminescence images and quantification of popliteal LN metastasis in nude mice after overexpressing circNCOR1 ($n = 12$ per group). **C,** Representative image of the popliteal LN in a nude mouse. **D,** Representative bioluminescence image of excised popliteal LNs from the nude mice ($n = 12$ per group). **E,** Representative images of anti-GFP IHC analysis of nude mice popliteal LNs ($n = 12$ per group). Red scale bars, 500 μm; black scale bar, 100 μm. **F,** The popliteal LN metastatic rates of the nude mice ($n = 12$ per group). **G** and **H,** Representative IHC images and percentages of LYVE-1–indicated lymphatic vessel density in footpad primary tumor tissues. Scale bars, 50 μm. The statistical difference was assessed with one-way ANOVA followed by Dunnett tests in **A**; and the two-tailed Student *t* test in **A**, **B**, **G**, and **H**; and the χ^2 test in **F**. Error bars show the SD from three independent experiments. **, $P < 0.01$. H&E, hematoxylin and eosin.

$DDX39B^{K53R}$ or SENP3 failed to restore the circNCOR1-induced inhibition of lymphangiogenesis (**Fig. 4H** and **I**). Taken together, our findings verify that SUMOylated DDX39B mediates circNCOR1 nuclear exportation to promote LN metastasis of bladder cancer.

circNCOR1 binds with hnRNPL

Considering that circNCOR1 nuclear exportation impairs its tumor-suppressive role, we believed that circNCOR1 functions primarily in the nucleus of bladder cancer cells. Many researchers have

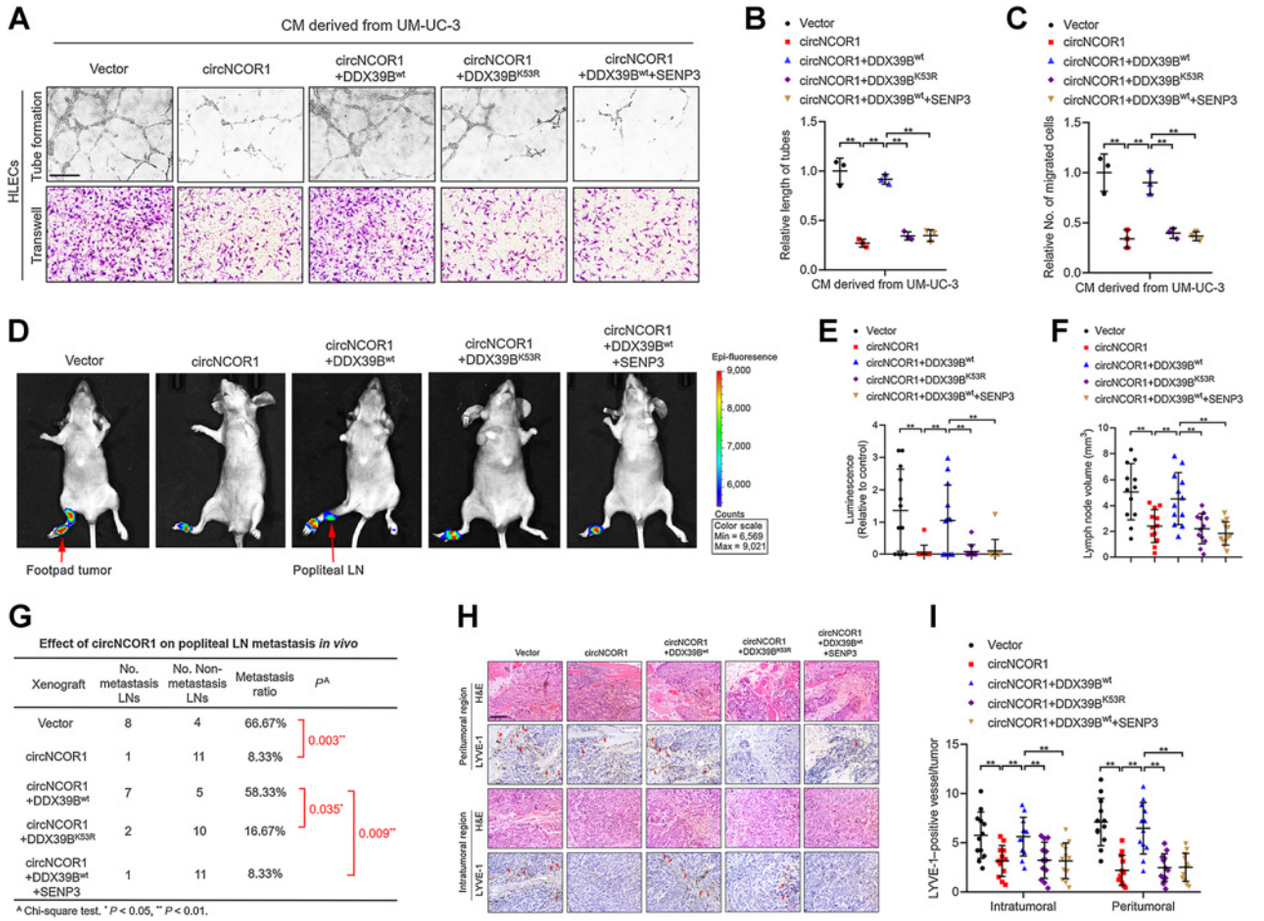

Figure 4.

SUMOylated DDX39B mediates circNCOR1 nuclear exportation to promote bladder cancer LN metastasis. **A–C,** Representative images (**A**) and quantification of the tube formation (**B**) and Transwell migration (**C**) of HLECs cocultured with UM-UC-3 cells. Scale bars, 100 μmol/L. **D–F,** Representative bioluminescence images (**D**) and quantification (**E** and **F**) of popliteal LN metastasis in the nude mice ($n = 12$ per group). **G,** The popliteal LN metastatic rate in the nude mice ($n = 12$ per group). **H** and **I,** Representative IHC images (**H**) and percentages (**I**) of LYVE-1–indicated lymphatic vessel density in the footpad primary tumor tissues from the nude mice. Scale bars, 100 μm. The statistical difference was assessed by one-way ANOVA followed by Dunnett tests in **B**, **C**, **E**, **F**, and **I**, and the χ^2 test in **G**. Error bars show the SD from three independent experiments. **, $P < 0.01$. H&E, hematoxylin and eosin.

proposed that nuclear circRNAs function by interacting with proteins (29, 30). Therefore, we performed RNA pull-down assay using biotinylated probes targeting the back-splicing site of circNCOR1 to detect the interacting proteins of circNCOR1. Silver staining revealed an obvious band with a molecular weight of 55 to 70 kDa in the biotinylated circNCOR1 group as compared with the control group (**Fig. 5A**), which mass spectroscopy identified as hnRNPL (**Fig. 5B**). Western blotting after RNA pull-down confirmed that circNCOR1 specifically enriched hnRNPL (**Fig. 5C**; Supplementary Fig. S5A–S5C). Consistently, RNA immunoprecipitation (RIP) assays using anti-hnRNPL verified significant enrichment of circNCOR1 compared with the IgG group (**Fig. 5D**; Supplementary Fig. S5D). FISH and immunofluorescence assays revealed circNCOR1 and hnRNPL colocalization in the nucleus of bladder cancer cells (**Fig. 5E**), indicating that circNCOR1 may function by binding with hnRNPL. To further analyze the specific interaction sites between circNCOR1 and hnRNPL, we used RBPmap, a website for mapping the binding sites of RNA-binding proteins, to identify a putative hnRNPL-binding motif located on the 80- to 130-nt region of circNCOR1 and that formed a stem-loop structure (**Fig. 5F** and **G**). Mutation of the circNCOR1 80- to 130-nt region significantly decreased circNCOR1 enrichment by hnRNPL (**Fig. 5H**; Supplementary Fig. S5E), suggesting that the 80- to 130-nt sequences are essential for circNCOR1–hnRNPL interaction.

circNCOR1 promotes SMAD7 transcription by recruiting hnRNPL

To investigate the downstream target genes of circNCOR1, we performed NGS (GSE190827), which revealed that a total of 741 genes were upregulated after overexpressing circNCOR1 in bladder cancer cells (**Fig. 5I**). Kyoto Encyclopedia of Genes and Genomes (KEGG) pathway enrichment analysis showed that the TGFβ signaling pathway was the most significantly enriched one from among 10 cancer-related signal transduction pathways (**Fig. 5J**). Then, we detected the expression profile of pivotal genes in the TGFβ signaling pathway. *SMAD7* was markedly upregulated in circNCOR1-overexpressing bladder cancer cells and was downregulated after knocking down circNCOR1 (**Fig. 5K**; Supplementary Fig. S5F–S5H). SMAD7 is an endogenous negative regulator of the TGFβ–SMAD signaling pathway, inhibiting

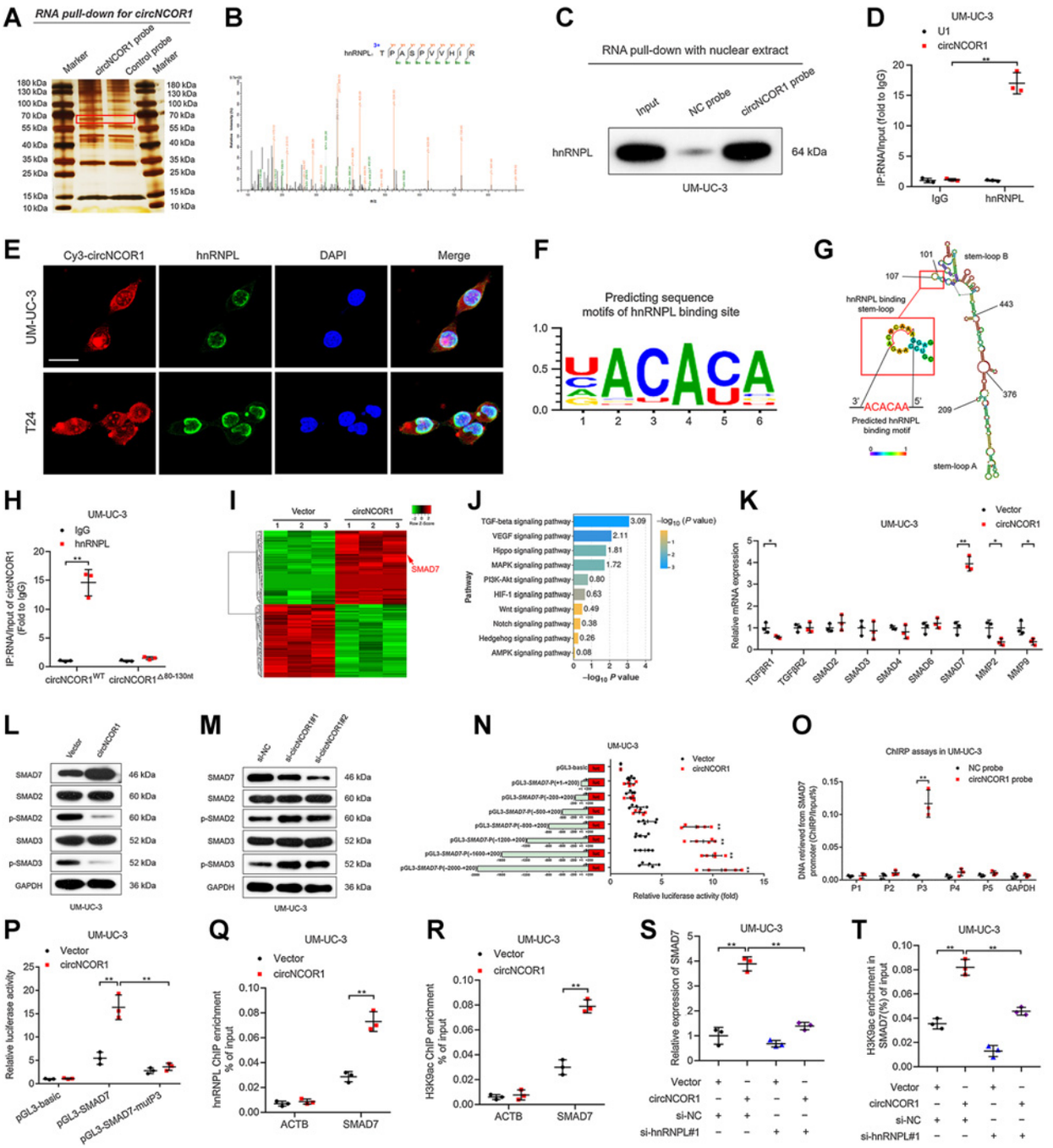

Figure 5.

circNCOR1 promotes *SMAD7* transcription by recruiting hnRNPL. **A,** Silver staining image of RNA pull-down assay with circNCOR1 and control probes. **B,** Mass spectrometry analysis of circNCOR1-binding proteins after RNA pull-down assay. **C,** Western blotting of the interaction between circNCOR1 and hnRNPL. **D,** RIP assays revealing circNCOR1 enrichment by hnRNPL in UM-UC-3 cells. **E,** Representative images of circNCOR1 and hnRNPL colocalization in bladder cancer cells. Scale bars, 5 μm. **F,** hnRNPL-binding motif predicted by RBPmap. **G,** The stem-loop structure of hnRNPL-binding motifs in circNCOR1. **H,** RIP assays after deletion of the 80- to 130-nt regions of circNCOR1 in UM-UC-3 cells. **I,** Heatmap of differentially expressed transcripts in circNCOR1-overexpressing UM-UC-3 cells. **J,** KEGG pathway enrichment analysis of the enriched pathways in circNCOR1-overexpressing UM-UC-3 cells. **K,** qRT-PCR analysis of TGFβ signaling pathway-related genes in circNCOR1-overexpressing UM-UC-3 cells. **L** and **M,** Western blotting of crucial proteins in the TGFβ–SMAD signaling pathway after circNCOR1 overexpression (**L**) or downregulation (**M**) in UM-UC-3 cells. **N,** Transcriptional activity of *SMAD7* in circNCOR1-overexpressing UM-UC-3 cells transfected with truncated *SMAD7* promoter luciferase plasmids. **O,** ChIRP assays detected the circNCOR1-associated chromatin fragments of the *SMAD7* promoter in UM-UC-3 cells. **P,** Luciferase activity in UM-UC-3 cells. **Q** and **R,** ChIP-qPCR of hnRNPL (**Q**) and H3K9ac (**R**) enrichment on *SMAD7* promoter after circNCOR1 overexpression in UM-UC-3 cells. **S,** qRT-PCR analysis of *SMAD7* expression in circNCOR1-overexpressing UM-UC-3 cells with or without silencing *hnRNPL*. **T,** ChIP-qPCR analysis of H3K9ac enrichment on *SMAD7* promoter in circNCOR1-overexpressing UM-UC-3 cells with or without silencing *hnRNPL*. The statistical difference was assessed by the two-tailed Student *t* test in **D**, **H**, **K**, **N**, **O**, **Q**, and **R**, and one-way ANOVA followed by Dunnett tests in **P**, **S**, and **T**. Error bars show the SD from three independent experiments. *, $P < 0.05$; **, $P < 0.01$.

the TGFβ receptor-mediated SMAD phosphorylation (31). Therefore, we performed Western blotting to confirm that circNCOR1-induced SMAD7 overexpression decreased phosphorylated SMAD2 (p-SMAD2) and SMAD3 (p-SMAD3) expression levels. Conversely, knocking down circNCOR1 obviously upregulated the p-SMAD2 and p-SMAD3 levels by downregulating SMAD7 expression (**Fig. 5L** and **M**; Supplementary Fig. S5I and S5J; Supplementary Fig. S6A–S6T). These data suggest that circNCOR1 inhibits the TGFβ–SMAD signaling pathway by upregulating SMAD7 expression.

To further explore the regulatory mechanism underlying circNCOR1-induced upregulation of SMAD7 expression, we constructed serial luciferase plasmids containing *SMAD7* promoter sequences of various lengths, i.e., -2000 nt to +200 nt. The promoter luciferase assays indicated that the -800-nt to -500-nt region of the *SMAD7* promoter markedly increased the luciferase activity in circNCOR1-overexpressing bladder cancer cells (**Fig. 5N**; Supplementary Fig. S7A), suggesting that this region is essential for circNCOR1-mediated *SMAD7* transactivation. As emerging studies have shown that circRNAs are similar to long noncoding RNAs in regulating the transcription of target genes by interacting with their promoters, the complementary regions between circNCOR1 and the *SMAD7* promoter were predicted by sequence alignment analysis (Supplementary Fig. S7B). The direct interaction between circNCOR1 and the -625-nt to -614-nt region (referred to as P3) of the *SMAD7* promoter was confirmed with chromatin isolation by RNA purification (ChIRP) assays (**Fig. 5O**; Supplementary Fig. S7C). Overexpressing circNCOR1 increased the luciferase activity of the *SMAD7* promoter in an obvious manner, while mutating the circNCOR1-binding region on the *SMAD7* promoter markedly decreased the circNCOR1-mediated transcriptional activation of *SMAD7* (**Fig. 5P**; Supplementary Fig. S7D), suggesting that circNCOR1 directly binds with the P3 region of the *SMAD7* promoter to form a DNA–RNA triplex and activate *SMAD7* transcription.

It is widely believed that histone modifications play a crucial role in the epigenetic regulation of gene expression, and we have previously reported that hnRNPL-induced histone modification contributes to the transcriptional activation of target genes (32, 33). Therefore, we further examined whether circNCOR1 promotes *SMAD7* transcription by recruiting hnRNPL to induce histone modification on *SMAD7* promoter. Chromatin immunoprecipitation (ChIP) assays showed that the enrichment of hnRNPL and histone H3K9 acetylation (H3K9ac) on *SMAD7* promoter were significantly increased in circNCOR1-overexpressing bladder cancer cells, while no obvious changes of other histone modification markers were observed, and silencing circNCOR1 impaired the enrichment of hnRNPL and H3K9ac status on *SMAD7* promoter (**Fig. 5Q** and **R**; Supplementary Fig. S7E–S7L). Moreover, ChIP analysis revealed that silencing hnRNPL significantly attenuated the circNCOR1 overexpression-induced SMAD7 transcriptional activity and H3K9ac enrichment on SMAD7 promoter (**Fig. 5S** and **T**; Supplementary Fig. S7M–S7P). Since the acetylation modification of histone was mainly catalyzed by histone acetyltransferases (HAT; ref. 34), we further performed co-IP analysis to confirm that p300, a HAT, interact with hnRNPL (Supplementary Fig. S7Q–S7S). Furthermore, treatment with C646, a specific p300 inhibitor, markedly impaired the circNCOR1-induced enrichment of H3K9ac on *SMAD7* promoter (Supplementary Fig. S7T and S7U), suggesting that circNCOR1-induced H3K9ac on *SMAD7* promoter is dependent of hnRNPL with the assistance of p300. Taken together, our results demonstrate that circNCOR1 activates *SMAD7* transcription by recruiting hnRNPL to increase p300-dependent H3K9ac on *SMAD7* promoter.

circNCOR1 inhibits LN metastasis of bladder cancer by inhibiting the TGFβ–SMAD signaling pathway

We explored whether the TGFβ–SMAD signaling pathway is essential for circNCOR1-inhibited lymphangiogenesis and LN metastasis of bladder cancer. Coculture with circNCOR1-overexpressing bladder cancer cells significantly inhibited HLECs tube formation and migration, while knocking down *SMAD7* rescued the ability of circNCOR1 overexpression to suppress HLECs tube formation and migration (**Fig. 6A–C**; Supplementary Fig. S8A–S8C). In addition, Transwell and wound healing assays confirmed that circNCOR1 overexpression attenuated bladder cancer cells migration and invasion, whereas knocking down *SMAD7* reversed the circNCOR1-mediated suppressive effect in an obvious manner (Supplementary Fig. S8D–S8G).

Then we implemented *in vivo* experiments to further examine the effect of circNCOR1-mediated *SMAD7* in bladder cancer LN metastasis. Downregulating *SMAD7* greatly increased the circNCOR1-induced reduction of the popliteal LN metastasis rate in nude mice (**Fig. 6D**). Moreover, knocking down *SMAD7* significantly attenuated the inhibition of bladder cancer cells metastasis to the popliteal LNs mediated by circNCOR1 overexpression (**Fig. 6E** and **F**). Therefore, our findings illustrate that circNCOR1 inhibits lymphangiogenesis and LN metastasis of bladder cancer by suppressing TGFβ–SMAD signaling pathway activation.

SUMOylated DDX39B inhibits circNCOR1-induced SMAD7 upregulation

We further examined whether SUMOylated DDX39B attenuates *SMAD7* expression by facilitating circNCOR1 nuclear exportation to promote bladder cancer LN metastasis. Luciferase assays showed that *DDX39B* overexpression induced circNCOR1 nuclear exportation and reduced the luciferase activity of the *SMAD7* promoter in circNCOR1-overexpressing bladder cancer cells. $DDX39B^{K53R}$ or SENP3 treatment rescued this inhibitory effect by retaining circNCOR1 in the nucleus (**Fig. 6G**; Supplementary Fig. S9A). Moreover, qRT-PCR verified that *DDX39B* overexpression significantly inhibited the circNCOR1-mediated upregulation of *SMAD7*, whereas $DDX39B^{K53R}$ or SENP3 treatment markedly reversed *SMAD7* expression (**Fig. 6H**; Supplementary Fig. S9B). Consistently, western blotting confirmed that DDX39B overexpression significantly inhibited circNCOR1-induced SMAD7 upregulation, whereas $DDX39B^{K53R}$ or SENP3 treatment markedly retrieved SMAD7 expression (**Fig. 6I** and **J**; Supplementary Fig. S9C and S9D). Taken together, these results demonstrate that SUMOylated DDX39B promotes circNCOR1 nuclear exportation to inhibit circNCOR1-induced SMAD7 upregulation.

circNCOR1 inhibits tumor growth in PDXs from LN metastatic bladder cancer

Since circNCOR1 plays a suppressive role in bladder cancer LN metastasis, we further established PDX models using tumor tissues from patients with LN metastatic bladder cancer to examine the therapeutic effect of circNCOR1. When the PDXs were 200 mm^3, the mice were injected intratumorally with *in vivo*–optimized circNCOR1 lentivirus or siSMAD7 reagent, and inhibited TGFβ/SMAD signaling pathway by treating with LY2157299, a TGFβ signaling inhibitor or *in vivo*–optimized siTGFBR1 reagent (**Fig. 7A**). Overexpression of circNCOR1 and inhibition of TGFβ/SMAD signaling pathway markedly suppressed the tumor volume growth in PDX models, while siSMAD7 exhibited opposite effect. Moreover, the tumor volume of PDXs in the mice that received circNCOR1 lentivirus combined with LY2157299 was obviously

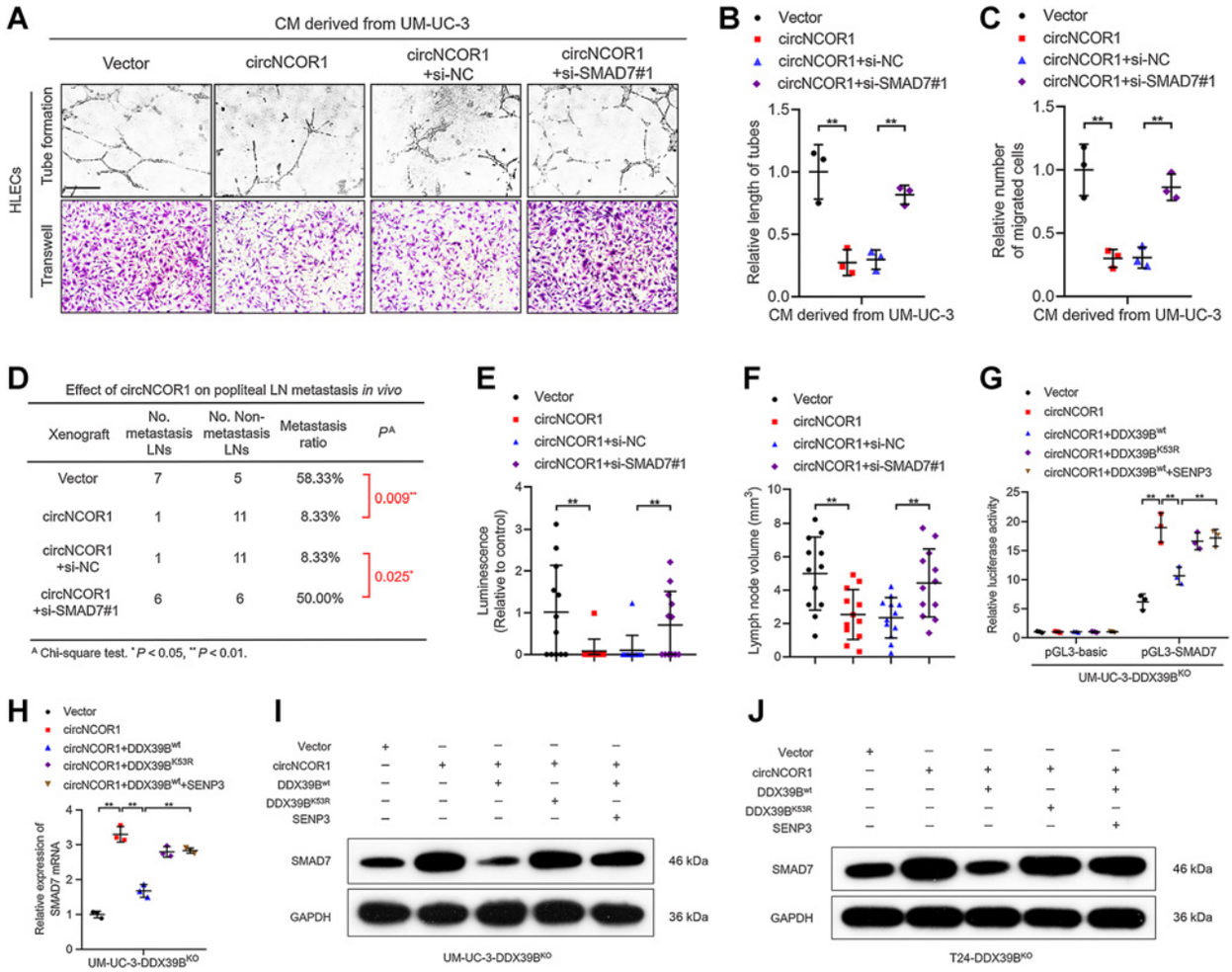

Figure 6.

circNCOR1 inhibits LN metastasis of bladder cancer by inhibiting the TGFβ–SMAD signaling pathway. **A–C,** Representative images (**A**) and quantification of the tube formation (**B**) and Transwell migration (**C**) by HLECs cocultured with UM-UC-3 cells. Scale bars, 100 μm. **D,** The popliteal LN metastatic rate in the nude mice ($n = 12$ per group). **E** and **F,** Bioluminescence (**E**) and LN volume (**F**) of popliteal LN metastasis in the nude mice ($n = 12$ per group). **G,** Luciferase activity of the *SMAD7* promoter in indicated UM-UC-3 cells. **H,** qRT-PCR analysis of *SMAD7* expression in indicated UM-UC-3 cells. **I** and **J,** Western blotting of SMAD7 expression in indicated UM-UC-3 (**I**) and T24 (**J**) cells. The statistical difference was assessed by the two-tailed Student *t* test in **B**, **C**, **E**, and **F**, and the χ^2 test in **D**; and one-way ANOVA followed by Dunnett tests in **G** and **H**. Error bars show the SD from three independent experiments. **, $P < 0.01$.

decreased compared with those in the mice treated with circNCOR1 lentivirus or LY2157299 alone (**Fig. 7B** and **C**; Supplementary Fig. S9E and S9F), indicating that circNCOR1 and LY2157299 have a synergistic therapeutic effect on bladder cancer progression. In addition, circNCOR1 lentivirus treatment significantly increased the circNCOR1 and *SMAD7* expression levels and suppressed the LYVE-1-indicated MLD in the PDXs (**Fig. 7D** and **E**; Supplementary Fig. S9G and S9H). Collectively, these results demonstrate that circNCOR1 has the potential to become a druggable inhibitor in bladder cancer therapy.

Clinical relevance of the DDX39B–circNCOR1–SMAD7 axis in patients with bladder cancer

To examine whether the DDX39B–circNCOR1–SMAD7 axis is clinically associated with lymphangiogenesis and bladder cancer LN metastasis, we first evaluated *DDX39B* expression in patients with bladder cancer. The results showed that *DDX39B* was markedly upregulated in bladder cancer tissues rather than in NATs (**Fig. 7F**; Supplementary Fig. S9I–S9K). *DDX39B* overexpression was related to the LN metastasis of patients with bladder cancer in our large clinical cohort (**Fig. 7G**). Furthermore, double immunofluorescent staining revealed a positive correlation between DDX39B expression and LYVE-1-indicated MLD in both the intratumoral and peritumoral region of bladder cancer tissues (**Fig. 7H–J**), indicating that DDX39B overexpression is associated with lymphangiogenesis of bladder cancer. Next, we explored the clinical correlation of circNCOR1-induced SMAD7 in our clinical cohort of 228 patients with bladder cancer. There was a positive correlation between circNCOR1 expression and SMAD7 levels in both bladder cancer tissues and paired NATs (**Fig. 8A–C**). Moreover, statistical analysis of the cohort verified that *SMAD7* was significantly downregulated in bladder cancer tissues as compared with NATs, consistent with the results from The Cancer Genome Atlas database (**Fig. 8D–F**; Supplementary Table S4). Kaplan–Meier analysis revealed that *SMAD7* was negatively related

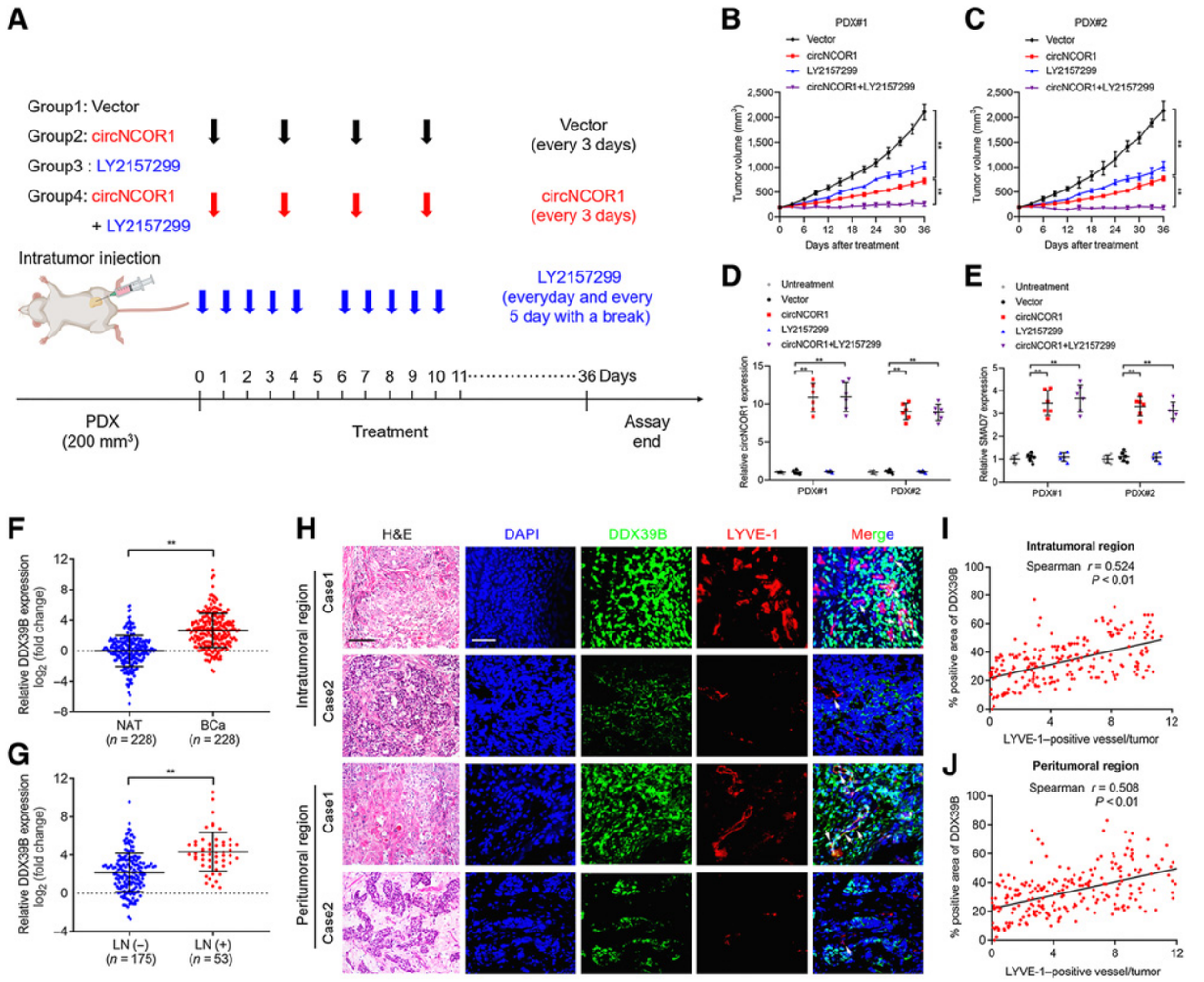

Figure 7.

circNCOR1 inhibits tumor growth in PDXs from LN metastatic bladder cancer. **A,** Timeline schematic for treatment of the mice carrying PDX. **B** and **C,** circNCOR1 and LY2157299 significantly inhibited PDXs growth in the mice ($n = 6$ per group). **D** and **E,** qRT-PCR analysis of circNCOR1 (**D**) and *SMAD7* (**E**) expression in PDXs before and after treatment ($n = 6$ per group). **F** and **G,** qRT-PCR of *DDX39B* expression in bladder cancer (BCa) tissues versus NATs (**F**) and LN-positive versus LN-negative bladder cancer tissues ($n = 228$; **G**). **H,** Representative images of DDX39B and LYVE-1–indicated lymphatic vessel density in bladder cancer tissues. H&E, hematoxylin and eosin. Scale bar, 100 μm. **I** and **J,** Correlation analysis of DDX39B expression and LYVE-1–indicated lymphatic vessel density in bladder cancer tissues ($n = 228$). The statistical difference was assessed by one-way ANOVA followed by Dunnett tests in **B–E** and the nonparametric Mann–Whitney *U* test in **F** and **G**. Error bars show the SD from three independent experiments. **, $P < 0.01$.

to poor prognosis in the patients with bladder cancer (**Fig. 8G** and **H**). Taken together, our results demonstrate that circNCOR1 inhibits LN metastasis of bladder cancer by upregulating *SMAD7* in a SUMOylated DDX39B-dependent manner.

Discussion

The nuclear exportation of RNA molecules is widely involved in activating prometastatic signaling, endowing tumor cells with an aggressive characteristic and stimulating tumor metastasis, which has emerged as a noticeable field of RNA-dependent tumor clinical therapy (35, 36). Yet, the biological role of circRNA nuclear exportation in LN metastasis of bladder cancer remains unknown. In the present study, we identified a nuclear translocated circRNA, circNCOR1, which is downregulated in bladder cancer and which correlated negatively with lymphangiogenesis and LN metastasis of bladder cancer. The nuclear exportation of circNCOR1 intensively impaired its ability for inhibiting TGFβ–SMAD signaling pathway activation to suppress bladder cancer LN metastasis. Moreover, we confirmed that promoting circNCOR1 nuclear retention achieved effective inhibition of bladder cancer lymphangiogenesis and popliteal LN metastasis *in vivo*. Therefore, our findings highlight the insight of circRNA nuclear exportation in regulating tumor metastasis and indicate that targeting circNCOR1 nuclear exportation may be a potential therapeutic strategy for LN metastatic bladder cancer (**Fig. 8I**).

DDX39B possesses a variety of PTMs that are crucial for recruiting RNA export complexes (37, 38). Nevertheless, the regulatory role of certain PTMs in DDX39B mediation of circRNA nuclear exportation remains unknown. In this study, we confirmed that DDX39B was

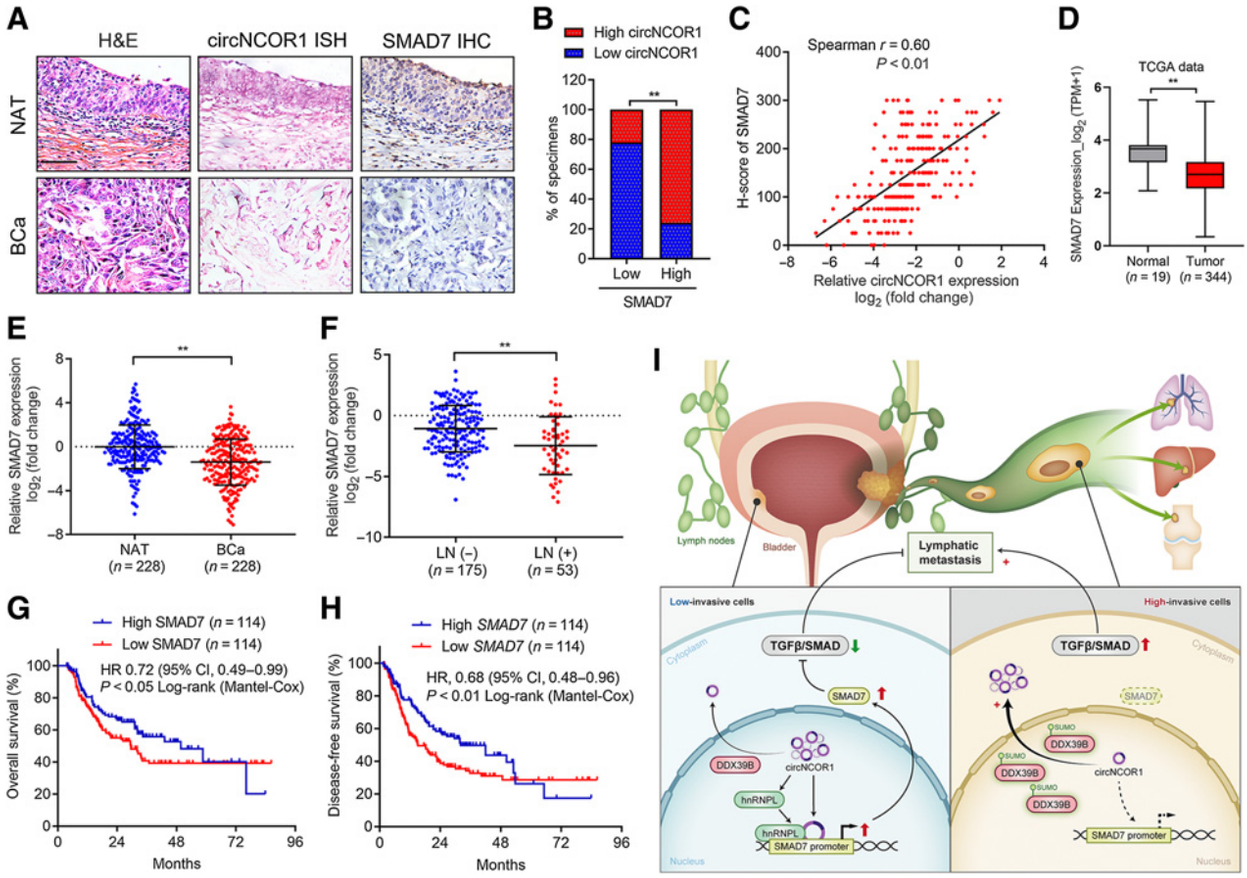

Figure 8.

Clinical relevance of the DDX39B–circNCOR1–SMAD7 axis in patients with bladder cancer. **A** and **B,** circNCOR1 expression correlated positively with SMAD7 expression in the bladder cancer tissues ($n = 228$). Scale bars, 50 μm. **C,** Correlation analysis of circNCOR1 and SMAD7 expression in bladder cancer tissues ($n = 228$). **D,** *SMAD7* expression levels were downregulated in bladder cancer tissues from The Cancer Genome Atlas (TCGA) database. **E,** qRT-PCR analysis of *SMAD7* expression in bladder cancer (BCa) tissues and NATs ($n = 228$). **F,** Comparison of *SMAD7* expression in LN-positive and LN-negative bladder cancer tissues. **G** and **H,** Kaplan–Meier survival analysis of the OS (**G**) and DFS (**H**) of patients with bladder cancer with low versus high *SMAD7* expression. The cutoff is the median. **I,** Schematic diagram describing that circNCOR1 activates *SMAD7* transcription by recruiting hnRNPL to increase H3K9ac on *SMAD7* promoter, thus inhibiting TGFβ–SMAD signaling pathway to suppress LN metastasis of bladder cancer, whereas SUMOylated of DDX39B promotes the nuclear exportation of circNCOR1 to impair the inhibitory role of circNCOR1 on bladder cancer LN metastasis. The statistical difference was assessed by the χ^2 test in **B** and the nonparametric Mann–Whitney *U* test in **D–H**. Error bars show the SD from three independent experiments. **, $P < 0.01$.

SUMOylated at the K53 residue and that the SUMOylation markedly enhanced the efficiency of DDX39B in mediating circNCOR1 nuclear exportation in bladder cancer cells. We found that overexpressing DDX39B alone had little effect on circNCOR1 nuclear exportation, while the conjugation of SUMO2 at the K53 residue dramatically enhanced DDX39B regulation of circNCOR1 nuclear exportation. Specifically, inhibiting DDX39B SUMOylation with the enzyme SENP3 dramatically impaired circNCOR1 nuclear–cytoplasmic transportation. Our results reveal a crucial mechanism by which DDX39B controls circRNA nuclear exportation in a SUMOylation-dependent manner, providing a new perspective on DDX39B mediation of circRNA nuclear–cytoplasmic trafficking.

RNA-seq analyses series have shed new light on a wide range of circRNAs and revealed that circRNAs with abnormal expression patterns contribute extensively to tumor stemness, EMT, and therapeutic resistance (39–41). circRNAs act as mediators of microRNA activity, scaffolds of protein complexes and inhibitors of RNA–protein interactions, thereby controlling the signaling cascade to regulate tumor metastasis (42–44). However, the regulatory mechanism of circRNAs for guiding epigenetic activation of gene transcription is largely unclear. Herein, we found that circRNAs could interact with the promoters of their target genes to serve as the "address code" of specific chromatin-modifying enzymes for gene transcriptional regulation, in which circNCOR1 directly bound with the *SMAD7* promoter to form a DNA–RNA triplex, increasing hnRNPL-induced H3K9ac to promote *SMAD7* transcription. Importantly, deleting the circNCOR1-binding sequence on the *SMAD7* promoter or muting the hnRNPL-interacting motif on circNCOR1 significantly impaired the circNCOR1-induced transcriptional activation of *SMAD7*. Our findings provide a new perspective for studying the regulatory mechanism underlying circRNA in mediating gene expression by recruiting histone-modifying enzymes to precisely locate on the gene promoters, thereby having an efficient, stable epigenetically transcriptional regulatory effect.

PDX models are created by directly transplanting tumor fragments surgically dissected from patients into immunodeficient mice and have become increasingly utilized as a promising tool for cancerous translational research (45, 46). Accumulating evidences have proposed that PDX models share similar pathohistologic and epigenetic features with their original tumor tissues and have emerged as a useful model for preclinical drug evaluation, biomarker exploration, and personalized medicine therapy (47, 48). Targeted delivery of noncoding RNA inhibitors and oligonucleotides by lipid nanoparticles or siRNA conjugates has broad potential as a therapeutic against cancer (49,50). Here, we established PDX models using LN metastatic bladder cancer tissues to perform therapeutic experiments, in which circNCOR1 lentivirus treatment significantly upregulated *SMAD7* expression and suppressed bladder cancer growth and tumor burden. We also performed experimental therapy with the TGFβ signaling inhibitor LY2157299 in the PDX models and found that it can also efficiently inhibit tumor volume growth. Importantly, combined treatment of circNCOR1 and LY2157299 exhibited a synergistic effect in impeding tumor progression in the PDXs. Our results provide comprehensive evidence that circNCOR1 serves as a tumor suppressor and propose circNCOR1 as a potential therapeutic inhibitor of bladder cancer.

In summary, our study highlights a novel mechanism underlying SUMOylation-induced nuclear exportation of circNCOR1 mediating the DDX39B–circNCOR1–SMAD7 axis to regulate lymphangiogenesis of bladder cancer. Furthermore, we demonstrate that blocking DDX39B SUMOylation restored the inhibitory effect of circNCOR1 on bladder cancer LN metastasis *in vivo*. These findings provide new understanding of the regulatory mechanism of SUMOylation-driven circRNA nuclear exportation to trigger lymphangiogenesis of bladder cancer, suggesting circNCOR1 as an encouraging therapeutic inhibitor for LN metastatic bladder cancer.

Authors' Disclosures

No disclosures were reported.

Authors' Contributions

M. An: Writing–original draft, project administration. **H. Zheng:** Project administration. **J. Huang:** Supervision. **Y. Lin:** Methodology. **Y. Luo:** Writing–original draft. **Y. Kong:** Investigation. **M. Pang:** Data curation, software. **D. Zhang:** Validation, investigation. **J. Yang:** Methodology. **J. Chen:** Visualization, methodology. **Y. Li:** Data curation, formal analysis. **C. Chen:** Conceptualization, writing–original draft. **T. Lin:** Conceptualization, writing–review and editing.

Acknowledgments

The authors thank Prof. Jinxin Zhang, Department of Medical Statistics and Epidemiology, School of Public Health, Sun Yat-sen University, for statistical advice and research comments. This study was funded by the National Key Research and Development Program of China (grant no. 2018YFA0902803), the National Natural Science Foundation of China (grant nos. 81825016, 81802530, 81871945, 81902589, 81772719, 81772728, 81972385, 82173272, 82103536, 82103416, 82173266, and U21A20383), the Guangdong Basic and Applied Basic Research Foundation (grant no. 2021A1515010355, 2021B1515020091, 2020A1515010815, and 2018B010109006), and the Science and Technology Program of Guangzhou, China (grant nos. 202002030388, 201803010049, and 2017B020227007).

The costs of publication of this article were defrayed in part by the payment of page charges. This article must therefore be hereby marked *advertisement* in accordance with 18 U.S.C. Section 1734 solely to indicate this fact.

Received December 19, 2021; revised February 28, 2022; accepted April 6, 2022; published first April 8, 2022.

References

1. Teoh JY, Huang J, Ko WY, Lok V, Choi P, Ng CF, et al. Global trends of bladder cancer incidence and mortality, and their associations with tobacco use and gross domestic product per capita. Eur Urol 2020;78:893–906.
2. Safiri S, Kolahi AA, Naghavi M, Global Burden of Disease Bladder Cancer Collaborators. Global, regional and national burden of bladder cancer and its attributable risk factors in 204 countries and territories, 1990–2019: a systematic analysis for the global burden of disease study 2019. BMJ Glob Health 2021;6:e004128.
3. Liedberg F, Mansson W. Lymph node metastasis in bladder cancer. Eur Urol 2006;49:13–21.
4. Leveridge MJ, Siemens DR, Mackillop WJ, Peng Y, Tannock IF, Berman DM, et al. Radical cystectomy and adjuvant chemotherapy for bladder cancer in the elderly: a population-based study. Urology 2015;85:791–8.
5. Liu S, Chen X, Lin T. Lymphatic metastasis of bladder cancer: Molecular mechanisms, diagnosis and targeted therapy. Cancer Lett 2021;505:13–23.
6. Zhu J, Luo Y, Zhao Y, Kong Y, Zheng H, Li Y, et al. circEHBP1 promotes lymphangiogenesis and lymphatic metastasis of bladder cancer via miR-130a-3p/TGFβR1/VEGF-D signaling. Mol Ther 2021;29:1838–52.
7. Zheng H, Chen C, Luo Y, Yu M, He W, An M, et al. Tumor-derived exosomal BCYRN1 activates WNT5A/VEGF-C/VEGFR3 feedforward loop to drive lymphatic metastasis of bladder cancer. Clin Transl Med 2021;11:e497.
8. Renyi-Vamos F, Tovari J, Fillinger J, Timar J, Paku S, Kenessey I, et al. Lymphangiogenesis correlates with lymph node metastasis, prognosis, and angiogenic phenotype in human non-small cell lung cancer. Clin Cancer Res 2005;11:7344–53.
9. Chen LL. The expanding regulatory mechanisms and cellular functions of circular RNAs. Nat Rev Mol Cell Biol 2020;21:475–90.
10. Wang L, Tong X, Zhou Z, Wang S, Lei Z, Zhang T, et al. Circular RNA hsa_circ_0008305 (circPTK2) inhibits TGF-β-induced epithelial-mesenchymal transition and metastasis by controlling TIF1γ in non-small cell lung cancer. Mol Cancer 2018;17:140.
11. Kong Y, Li Y, Luo Y, Zhu J, Zheng H, Gao B, et al. circNFIB1 inhibits lymphangiogenesis and lymphatic metastasis via the miR-486–5p/PIK3R1/VEGF-C axis in pancreatic cancer. Mol Cancer 2020;19:82.
12. Li Z, Huang C, Bao C, Chen L, Lin M, Wang X, et al. Exon-intron circular RNAs regulate transcription in the nucleus. Nat Struct Mol Biol 2015;22:256–64.
13. Noh JH, Kim KM, McClusky WG, Abdelmohsen K, Gorospe M. Cytoplasmic functions of long noncoding RNAs. Wiley Interdiscip Rev RNA 2018;9:e1471.
14. Zhou M, Xiao MS, Li Z, Huang C. New progresses of circular RNA biology: from nuclear export to degradation. RNA Biol 2021;18:1365–73.
15. Nachmias B, Schimmer AD. Targeting nuclear import and export in hematological malignancies. Leukemia 2020;34:2875–86.
16. Chao F, Song Z, Wang S, Ma Z, Zhuo Z, Meng T, et al. Novel circular RNA circSOBP governs amoeboid migration through the regulation of the miR-141–3p/MYPT1/p-MLC2 axis in prostate cancer. Clin Transl Med 2021;11:e360.
17. Chen RX, Chen X, Xia LP, Zhang JX, Pan ZZ, Ma XD, et al. N(6)-methyladenosine modification of circNSUN2 facilitates cytoplasmic export and stabilizes HMGA2 to promote colorectal liver metastasis. Nat Commun 2019;10:4695.
18. Shen H. UAP56- a key player with surprisingly diverse roles in pre-mRNA splicing and nuclear export. BMB Rep 2009;42:185–8.
19. Gatfield D, Le Hir H, Schmitt C, Braun IC, Köcher T, Wilm M, et al. The DExH/D box protein HEL/UAP56 is essential for mRNA nuclear export in Drosophila. Curr Biol 2001;11:1716–21.
20. Huang C, Liang D, Tatomer DC, Wilusz JE. A length-dependent evolutionarily conserved pathway controls nuclear export of circular RNAs. Genes Dev 2018;32:639–44.
21. Wan Y, Hopper AK. Size matters: conserved proteins function in length-dependent nuclear export of circular RNAs. Genes Dev 2018;32:600–1.
22. Li Z, Kearse MG, Huang C. The nuclear export of circular RNAs is primarily defined by their length. RNA Biol 2019;16:1–4.
23. Pühringer T, Hohmann U, Fin L, Pacheco-Fiallos B, Schellhaas U, Brennecke J, et al. Structure of the human core transcription-export complex reveals a hub for multivalent interactions. eLife 2020;9:e61503.

24. Shi P, Guo Y, Su Y, Zhu M, Fu Y, Chi H, et al. SUMOylation of DDX39A alters binding and export of antiviral transcripts to control innate immunity. J Immunol 2020;205:168–80.
25. Chen C, Luo Y, He W, Zhao Y, Kong Y, Liu H, et al. Exosomal long noncoding RNA LNMAT2 promotes lymphatic metastasis in bladder cancer. J Clin Invest 2020;130:404–21.
26. Fossati N, Willemse PM, Van den Broeck T, van den Bergh RCN, Yuan CY, Briers E, et al. The benefits and harms of different extents of lymph node dissection during radical prostatectomy for prostate cancer: a systematic review. Eur Urol 2017;72:84–109.
27. Yang Q, Li F, He AT, Yang BB. Circular RNAs: expression, localization, and therapeutic potentials. Mol Ther 2021;29:1683–702.
28. Chen C, Zheng H, Luo Y, Kong Y, An M, Li Y, et al. SUMOylation promotes extracellular vesicle-mediated transmission of lncRNA ELNAT1 and lymph node metastasis in bladder cancer. J Clin Invest 2021;131:e146431.
29. Huang A, Zheng H, Wu Z, Chen M, Huang Y. Circular RNA-protein interactions: functions, mechanisms, and identification. Theranostics 2020;10:3503–17.
30. Zhou WY, Cai ZR, Liu J, Wang DS, Ju HQ, Xu RH. Circular RNA: metabolism, functions and interactions with proteins. Mol Cancer 2020;19:172.
31. Ikushima H, Miyazono K. TGFbeta signalling: a complex web in cancer progression. Nat Rev Cancer 2010;10:415–24.
32. Zhao Z, Shilatifard A. Epigenetic modifications of histones in cancer. Genome Biol 2019;20:245.
33. Chen C, He W, Huang J, Wang B, Li H, Cai Q, et al. LNMAT1 promotes lymphatic metastasis of bladder cancer via CCL2 dependent macrophage recruitment. Nat Commun 2018;9:3826.
34. Grunstein M. Histone acetylation in chromatin structure and transcription. Nature 1997;389:349–52.
35. Hautbergue GM. RNA nuclear export: from neurological disorders to cancer. Adv Exp Med Biol 2017;1007:89–109.
36. Azizian NG, Li Y. XPO1-dependent nuclear export as a target for cancer therapy. J Hematol Oncol 2020;13:61.
37. Xiong F, Lin Y, Han Z, Shi G, Tian L, Wu X, et al. Plk1-mediated phosphorylation of UAP56 regulates the stability of UAP56. Mol Biol Rep 2012;39:1935–42.
38. Szymura SJ, Bernal GM, Wu L, Zhang Z, Crawley CD, Voce DJ, et al. DDX39B interacts with the pattern recognition receptor pathway to inhibit NF-kappaB and sensitize to alkylating chemotherapy. BMC Biol 2020;18:32.
39. Zhao Y, Zheng R, Chen J, Ning D. CircRNA CDR1as/miR-641/HOXA9 pathway regulated stemness contributes to cisplatin resistance in non-small cell lung cancer (NSCLC). Cancer Cell Int 2020;20:289.
40. Shang BQ, Li ML, Quan HY, Hou PF, Li ZW, Chu SF, et al. Functional roles of circular RNAs during epithelial-to-mesenchymal transition. Mol Cancer 2019;18:138.
41. Xu J, Ji L, Liang Y, Wan Z, Zheng W, Song X, et al. CircRNA-SORE mediates sorafenib resistance in hepatocellular carcinoma by stabilizing YBX1. Signal Transduct Target Ther 2020;5:298.
42. Zhu Z, Huang J, Li X, Xing J, Chen Q, Liu R, et al. Gut microbiota regulate tumor metastasis via circRNA/miRNA networks. Gut microbes 2020;12:1788891.
43. Li B, Zhu L, Lu C, Wang C, Wang H, Jin H, et al. circNDUFB2 inhibits non-small cell lung cancer progression via destabilizing IGF2BPs and activating anti-tumor immunity. Nat Commun 2021;12:295.
44. Ding L, Zhao Y, Dang S, Wang Y, Li X, Yu X, et al. Circular RNA circ-DONSON facilitates gastric cancer growth and invasion via NURF complex dependent activation of transcription factor SOX4. Mol Cancer 2019;18:45.
45. Yoshida GJ. Applications of patient-derived tumor xenograft models and tumor organoids. J Hematol Oncol 2020;13:4.
46. Hidalgo M, Amant F, Biankin AV, Budinská E, Byrne AT, Caldas C, et al. Patient-derived xenograft models: an emerging platform for translational cancer research. Cancer Discov 2014;4:998–1013.
47. Tentler JJ, Tan AC, Weekes CD, Jimeno A, Leong S, Pitts TM, et al. Patient-derived tumour xenografts as models for oncology drug development. Nat Rev Clin Oncol 2012;9:338–50.
48. Inoue T, Terada N, Kobayashi T, Ogawa O. Patient-derived xenografts as in vivo models for research in urological malignancies. Nat Rev Urol 2017;14:267–83.
49. Kanasty R, Dorkin JR, Vegas A, Anderson D. Delivery materials for siRNA therapeutics. Nat Mater 2013;12:967–77.
50. Matsui M, Corey DR. Non-coding RNAs as drug targets. Nat Rev Drug Discovery 2017;16:167–79.